*Materials Transactions*, Vol. 60, No. 7 (2019) pp. 1151 to 1158
Special Issue on Severe Plastic Deformation for Nanomaterials with Advanced Functionality

**Review**

# Strain Induced Segregations in Severely Deformed Materials

Xavier Sauvage*, Amandine Duchaussoy and Ghenwa Zaher

*Normandie Univ, UNIROUEN, INSA Rouen, CNRS, Groupe de Physique des Matériaux, 76000 Rouen, France*

Severely deformed materials intrinsically contain a large density of crystalline defects like dislocations or boundaries. The interactions between solute atoms or impurities with these defects play a key role in the grain refinement mechanisms as they affect dynamic recovery. This short review manuscript focusses on grain boundary segregations resulting from severe plastic deformation. The important contribution of atom probe tomography for the quantitative characterization of such segregations in various metallic alloys is at first highlighted. Then, a special emphasis is given on the physical mechanisms leading to strain induced segregations and on the connection that is sometimes observed with dynamic precipitation during severe plastic deformation. The last section is devoted to the influence of such grain boundary segregations in ultrafine grained alloys on the mechanical properties and on the thermal stability. [doi:10.2320/matertrans.MF201919]

(Received February 7, 2019; Accepted March 7, 2019; Published May 31, 2019)

***Keywords:*** *segregations, severe plastic deformation, metallic alloys, grain boundaries, crystalline defects, diffusion, precipitation, mechanical strength*

## 1. Introduction

Severe plastic deformation (SPD) has been successfully applied during the past twenty years to produce ultrafine grained (UFG) metallic materials.[1–3] A large number of processes have been developed, including some tentative up-scaling with envisioned applications where high strength materials are required. Indeed, the typical UFG structures achieved with such processes usually exhibit a grain size in a range of 50 to 500 nm with a major proportion of High Angle Grain Boundaries (HAGB). Then, according to the well-known Hall-Petch law,[4] such grain refinement leads to a significant increase of the yield stress as compared to coarse grained conventional alloys. For example, the tensile strength of SPD processed Al alloys might be over one GPa.[5–8] Beyond problems connected to the up-scaling of processes, one of the major limitations for applications is the low ductility that usually results from the very limited strain hardening capability of UFG alloys achieved by SPD. Therefore, various strategies have been proposed to tackle this issue.[9]

On a very practical point of view, one should admit that in spite of the huge amount of work carried out in the field, it is rather difficult to predict and to accurately control the grain size achieved by SPD. The influence of processing parameters like strain level, strain path, temperature, strain rate have been widely investigated and it provided an excellent basis to understand the grain refinement mechanisms. It is now well accepted that the huge dislocation densities produced during SPD reorganize at first leading to the formation of Low Angle Grain Boundaries (LAGBs). Then, further deformation introduces additional dislocations which progressively increases disorientation angles, leading to HAGBs. Finally, the balance between the creation of new dislocations and recovery processes gives rise to a steady state regime where the UFG structure does not significantly evolves anymore with further deformation.[10] It should be noted that the resulting Grain Boundaries (GBs) exhibit some specific features as compared to GBs observed in conventionally recrystallized materials. They are called "non-equilibrium" boundaries by some authors as they are characterized by a large density of intrinsic defects giving rise to local stress fields.[3,11] As a result, the investigation of such GBs has often demonstrated that their properties are significantly different like for example, a fastest GB diffusion.[12]

Since the grain size refinement mechanisms are controlled by the production and the cooperative recovery of defects and especially dislocations, then it is quite natural to understand that the material chemistry should play an important role due to the possible interaction between solutes and these defects. As soon as the early time of research on SPD materials, it has been shown indeed that for example, a small amount of Mg in solid solution in Al leads to a dramatic reduction of the grain size achieved by SPD.[13,14] This feature is illustrated on Fig. 1 where the grain size in the commercially pure Aluminum processed by HPT up to shear strain of about 700 (in the saturation regime) at room temperature (RT) is about 500 nm (Fig. 1(a)), while it is down to only 200 nm in the Al2 mass%Mg alloy processed in similar conditions (Fig. 1(b)). Similar features have been reported for Cu alloys,[15] or steels.[16,17] In some cases, the influence of a small amount of solute atoms is really impressive, like in the Cu–Sn system where the addition of only about 4 at% leads to a huge difference (grain size of 250 nm versus 70 nm) between the commercially pure Cu and the Cu–8 mass%Sn (Fig. 1(c) and 1(d)).

It has been proposed by some authors that the steady state grain size achieved by SPD was directly connected to the Stacking Fault Energy (SFE) that controls the dynamic recovery processes.[18] However, it has been recently demonstrated that even if alloying elements affect the SFE, there is no systematic correlation.[15,19] Besides, it is interesting to note that not only alloying elements but also a small amount of impurities might significantly affect the UFG structure achieved by SPD, as demonstrated by Zhang and co-authors for nickel[20,21] or Edalati and co-authors in aluminum.[22] Thus, as proposed by Edalati and co-authors,[19] mechanisms are obviously mainly controlled by the solute/defects interactions. This view is supported by recent work on strain induced grain boundary motion which is major

*Corresponding author, E-mail: xavier.sauvage@univ-rouen.fr

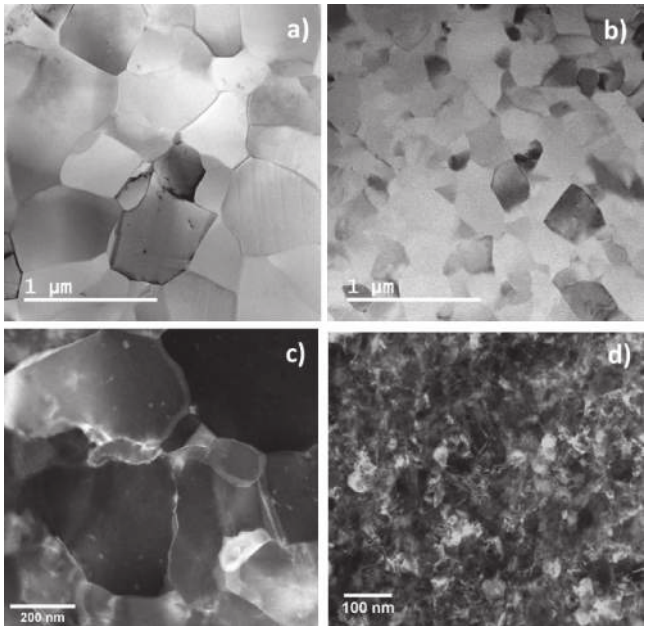


Fig. 1 STEM BF images of commercially pure Al (99.5%) (a) and Al–2 mass%Mg alloy (b) processed by HPT at RT (shear strain ~ 700). STEM DF images of commercially pure Cu (99.5%) (c) and Cu–8 mass%Sn alloy (d) processed by HPT at RT (shear strain ~ 1000).

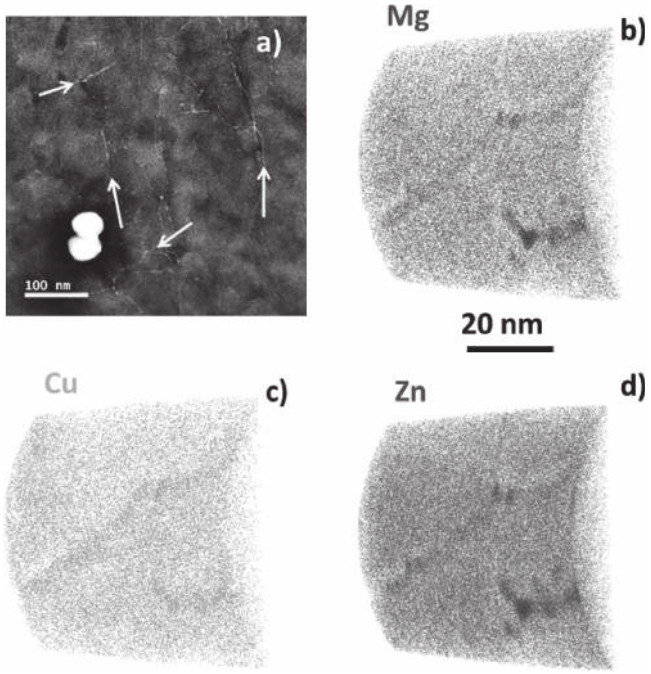


Fig. 2 7449 Aluminum alloy processed by HPT at RT (shear strain ~ 300). STEM HAADF image where GB segregations are arrowed (a), 3D reconstruction of a volume analyzed by APT showing that all major alloying elements have segregated at GBs (Mg (b), Cu (c) and Zn (d)).

phenomena occurring during SPD.[23,24] Thus, like during classical grain growth,[25] the interaction between solutes (or impurities) and GBs might significantly modify their energy and mobility and thus the microstructure resulting from SPD. This effect is of course more pronounced in case of GB segregations which is a frequent feature in metallic alloys processed by SPD as it will be shown in the following section. It is partly connected to the specificity of the "non-equilibrium" state of the GBs obtained during grain refinement by SPD,[17] but also related to solute drag by crystalline defects such as vacancies, dislocations and moving boundaries.[26] The influence of such segregations on mechanical properties and on the thermal stability of UFG alloys processed by SPD will be also discussed in the last section of this manuscript.

## 2. Experimental Evidences of SPD Induced GB Segregations

GB segregations play a major role on mechanical behavior of metallic alloys as they could affect for example creep properties, toughness, hydrogen embrittlement, grain growth, corrosion properties, ….[27] Equilibrium GB segregations are usually driven by a minimization of the GB energy, thus they could help stabilizing UFG microstructure by reducing the driving force for grain growth.[28–32] The Atom probe Tomography (APT) technique[33] which provides three dimensional reconstructions near the atomic resolution with a high chemical sensitivity is a key tool for the investigation of GB segregations.[34] It has also been shown that it could be successfully combined with Transmission Electron Microscopy (TEM) to correlate GB misorientation and the interfacial Gibbs excess free energy.[35]

Figure 2 exhibits typical segregations in a 7449 aluminum alloy processed by HPT at room temperature. These segregations are visualized over a relatively large field of view (Fig. 2(a)) by High Angle Annular Dark Field Scanning Transmission Electron Microscopy (HAADF-STEM). The z-contrast provided by this image indicates that Cu and Zn which have an atomic number significantly larger than Al, have segregated along some of the GBs. However, it does not allow straightforward and precise quantification of these segregations, for two main reasons: first because of GB roughness, curvature or tilt within the thin foil thickness and second because of the relatively limited chemical sensitivity of the analytical capability of the STEM. APT analyses provide a field of view that is much more limited but can reveal the complex grain boundary morphology and is sensitive to any chemical fluctuations with a somewhat similar sensitivity for all chemical elements (Fig. 2(a), 2(b) and 2(c)). Such GB segregations have been observed in most of Al alloys, including commercial 7### AA[5,6,8,36,37] or 6### AA,[38,39] binary Al–Zn,[40,41] Al–Cu,[42] Al–Mg[11,17,43,44] or aluminum alloyed with rare earth elements.[45] In these metallic materials, segregated elements are substitutional atoms and similarly segregation of Si at GBs has been reported in stainless steels processed by SPD.[46,47] It is however interesting to note that solutes or impurities that usually lie on interstitial sites of the crystal lattice could also be prone to GB segregation during SPD. It is the typical case of carbon in ferritic steels,[17] oxygen in Ti alloys[48] and carbon or oxygen in nickel.[49] One should note that even if the equilibrium solubility of carbon is relatively low in the bcc ferrite, it has been shown that severe plastic deformation could lead to the dissolution of carbides ($Fe_3C$),[50] leading to a strong carbon supply and extensive carbon segregations along GBs and the stabilization of nanoscaled ferrite with a grain size of only about 20 nm.[16]

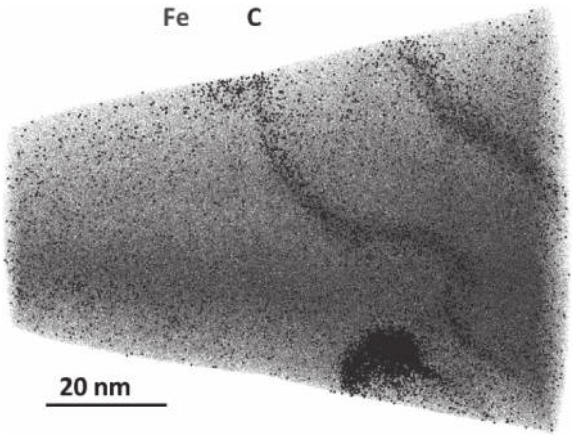


Fig. 3 3D reconstruction of a volume ($55 \times 55 \times 70\,nm^3$) analyzed by APT in a Fe–0.45%C steel processed by HPT at 350°C (shear strain ~ 300). Fe atoms are displayed in blue and C atoms in red to exhibit carbon segregations along GBs (the nanoscaled particle located at the bottom of the image is a cementite particle).

Such phenomenon is depicted in the Fig. 3 where the volume that has been analyzed by APT in a low carbon steel processed by HPT is displayed. A 10 nm carbon rich particle is located at the bottom of the image; it results from the fragmentation of the original cementite ($Fe_3C$) during SPD. This fragmentation leads to a partial dissolution of the $Fe_3C$ phase, and the carbon released in the bcc ferrite matrix segregates along crystalline defects and especially along boundaries (two of them appear in the image of the Fig. 3).

## 3. Mechanisms of Strain Induced Diffusion in Alloys Processed by Severe Plastic Deformation and Influence on Dynamic Precipitation

### 3.1 Fundamental mechanisms

Materials processed by SPD are characterized by high dislocation densities,[3] "non-equilibrium" grain boundaries[11] and high vacancy concentrations.[51,52] All these defects may influence the atomic mobility: dislocations could drag solutes[53] or act as diffusion pipes;[54] GBs are also fast diffusion paths[12] and could drag solute when they move during the deformation,[23,24,42] and at last, strain induced vacancies will directly enhance the atomic diffusion.[27] These respective contributions have been reviewed in Ref. 26 and will be shortly described in the following on the basis of experimental data reported for some aluminum alloys.

It has been reported that processing of Al–Mg solid solutions by High Pressure Torsion (HPT) leads to extensive GB segregations of Mg. It is interesting to note that such phenomenon occurs even if the Mg content is relatively low (2 mass%) and even if deformation is carried out at 200°C where the solid solution is supposed to be quite stable.[43,44] On the basis of experimental data, the atomic mobility of Mg atoms during SPD has been evaluated and the corresponding diffusion coefficients compared with classical bulk diffusion data (Fig. 4(a)). It clearly indicates that at room temperature the atomic mobility is strongly enhanced under SPD conditions (several orders of magnitude difference). Since Mg atoms diffusion is controlled by a vacancy mechanism, strain induced vacancies have been considered

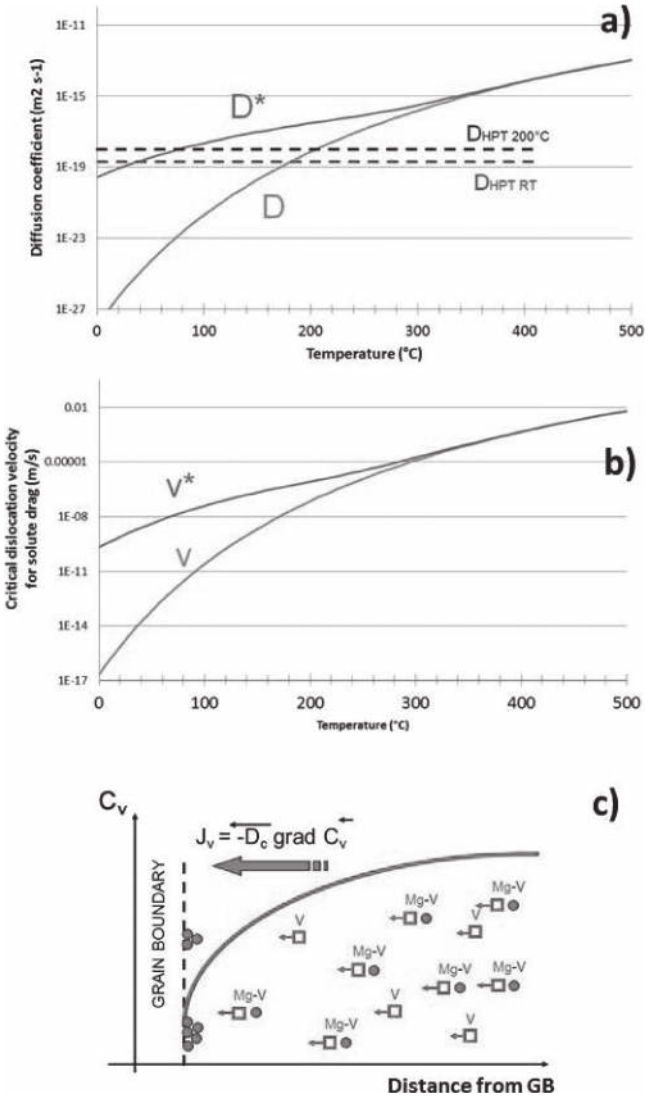


Fig. 4 (a) Diffusion coefficient D of Mg in Al as a function of temperature, and diffusion coefficient estimated taken into account strain induced vacancies (concentration $10^{-5}$) D* compared with experimental values estimated from experimental data after HPT at RT and at 200°C; (b) critical dislocation velocity V (and V* taken into account strain induced vacancies) for solute drag of Mg in Al; (c) schematic representation of Mg migration toward GBs in Al assisted by the flux of strain induced vacancies and resulting from the positive binding to vacancies (reproduced from Ref. 43 with permission from Elsevier).

for the calculation of the effective diffusion coefficient (D*). Experimental data seem to fit relatively well theoretical estimations if a concentration of strain induced vacancies of $10^{-5}$ is considered during SPD which is close to the values reported in the literature.[51] There could be however as well a significant contribution of dislocations, especially because in the Al–Mg system there are strong interactions between Mg and dislocations. However, as shown on Fig. 4(b), the critical dislocation velocity calculated for solute drag by moving dislocation stands always well below $10^{-4}$ m/s which is the lower bound estimated for the experimental conditions considered (see Ref. 43 for details). Thus, in this context, strain induced vacancies seem to play a key role in the formation of GB segregations during SPD. However, considering that they are continuously created during SPD[55] and annihilated on sinks that are GBs, a vacancy flux towards

GBs should proceed during SPD. Then, due to the positive binding energy of Mg atoms with vacancies in fcc Al, a flux of Mg atoms is created in the same direction leading to non-equilibrium GB segregations of Mg. This scenario schematically represented on Fig. 4(c) is rather similar to mechanisms reported in irradiated materials where a high concentration of point defects is also continuously created.[30,56] It may also account for the relatively high Mg concentrations that has been experimentally measured at GB by APT (up to 20 at% after SPD at RT[43]).

More recently, it has been demonstrated that GB segregations start appearing in the early stage of the grain refinement process by SPD in the Al–Cu system.[42] It has been then proposed that in this case, the solute drag by moving boundaries should be the major mechanism leading the GB segregations and as it will be discussed in the following it strongly promotes the strain induced decomposition of the solid solution and precipitation.

### 3.2 Connection with strain induced precipitation

There are situations where SPD leads to mechanical mixing and the formation of super saturated solid solutions in multi-phase metallic alloys,[57,58] but there are also situations where super saturated solid solutions decompose during SPD.[41,42,59,60] In the latter case, the initial material is single phase and the super saturated solid solution is usually obtained by quenching from high temperature where it is stable. In classical precipitate hardening alloys, the precipitation is achieved in a second step using thermal aging at relatively low temperature where there is enough atomic mobility and a maximum driving force for precipitation.[27] It has been found however that during SPD at room temperature (RT) some strain induced dynamic precipitation may occur for example in the Al–Zn,[41,59–61] and Al–Cu[42,62] binary systems. Of course, the slight increase of temperature during HPT might promote the atomic diffusion, but in fact it has been proven that this temperature increase is typically only 10 to 20°C in usual processing conditions (rotation speed of 1 rev/min or less).[63,64] The resulting enhanced atomic mobility cannot account for the fast phase separation that is observed experimentally in these systems at RT and the role of SPD induced crystalline defects is predominant.

The Bright Field STEM (BF-STEM) image in Fig. 5(a) shows the typical UFG structure of a solutionized Al–30Zn alloy processed by HPT at room temperature. Al (bright) and Zn (dark) grains are in a range of 200 to 500 nm and there are also few Zn particles that have nucleated inside Al grains. Extensive Zn GB segregations have been reported for this alloy.[41,59,60] Then, since GBs are fast diffusion paths,[12] these segregations provide a strong flux of Zn toward particles that nucleate at triple lines in the early stage of deformation. Thus, as schematically represented on Fig. 5(b), grain boundary segregations dramatically promote the dynamic precipitation process and at the end deeply affect the final UFG structure. It is interesting to note that a very similar mechanism has been observed in the Al–Cu system[42,62] where heterogeneous precipitation of the $Al_2Cu$ phase at GBs has been reported. However, in more complex aluminum alloys where interactions between solutes are strong, like AlMgZnCu[8,36,37] or AlMgCu[65] or AlMgSi,[38] even if GB segregations and dynamic precipitation occur, most of solutes are kept in solid solution inside ultrafine grains.

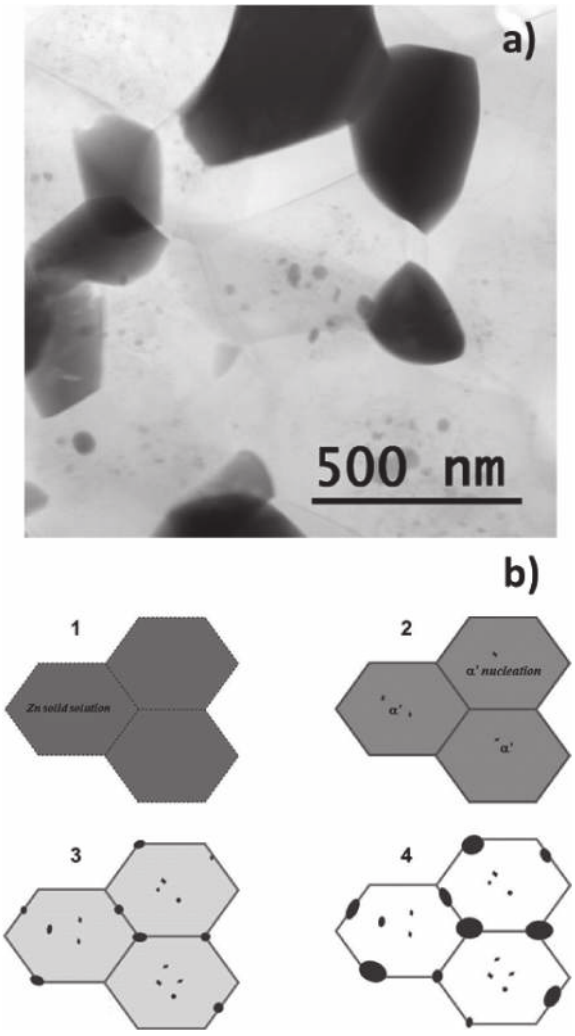


Fig. 5 Al–30Zn alloy processed by HPT at RT starting from a homogeneous solid solution; (a) STEM-BF image showing the strain induced precipitation (Zn grains and particles in dark); (b) schematic representation of the progressive mechanism leading to the phase separation: 1- initial solid solution, 2- precipitation of Zn rich particle ($\alpha'$) in grain interiors and GB segregations, 3- heterogeneous precipitation of Zn rich particles at GBs and triple lines, 4- particle coarsening, end of the phase separation with a matrix depleted in Zn (reproduced from Ref. 60 with permission from Wiley).

## 4. Influence of Strain Induced Segregations on Mechanical Properties and on Thermal Stability

### 4.1 Influence of strain induced segregations on mechanical properties

The high strength of UFG metallic alloys obtained by SPD processes originates mainly from the GB strengthening via the well-known Hall-Petch law.[4] Thus, it seems relatively natural to imagine that the occurrence of GB segregations might affect, at least in some cases, the mechanical strength of these materials. In nanocrystalline materials prepared by electrodeposition or sputtering, it has been shown that segregations often promote the strength.[66–68] The conclusions rose from such experimentally data have been also confirmed by first principle or MD simulations.[69,70]

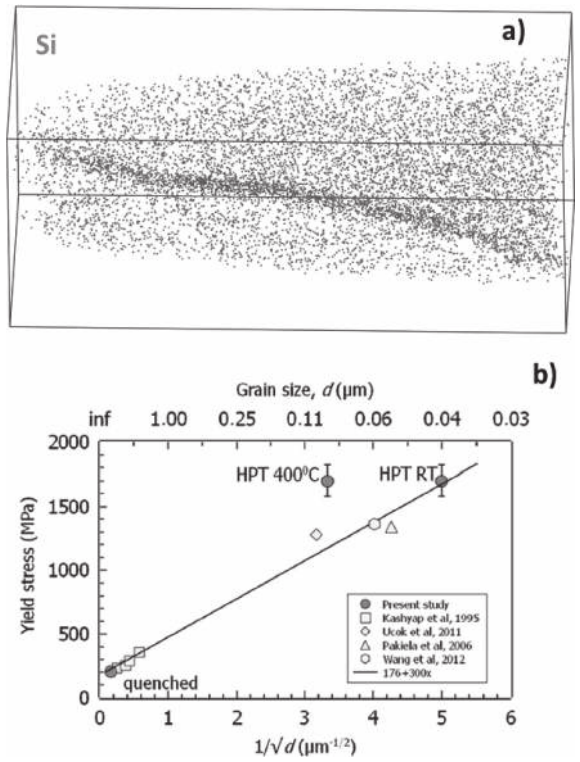


Fig. 6 (a) 3D reconstruction ($25 \times 25 \times 65\,nm^3$) of a volume analyzed in a 316 stainless steel processed by HPT at 400°C. Only Si atoms are plotted to exhibit the segregation along a GB. (b) Hall-Petch plot showing a significant deviation of the yield stress of this alloy comparing to the expected value. This phenomenon is attributed to the GB segregations that were not observed after HPT at RT (reproduced from Ref. 46 with permission from Elsevier).

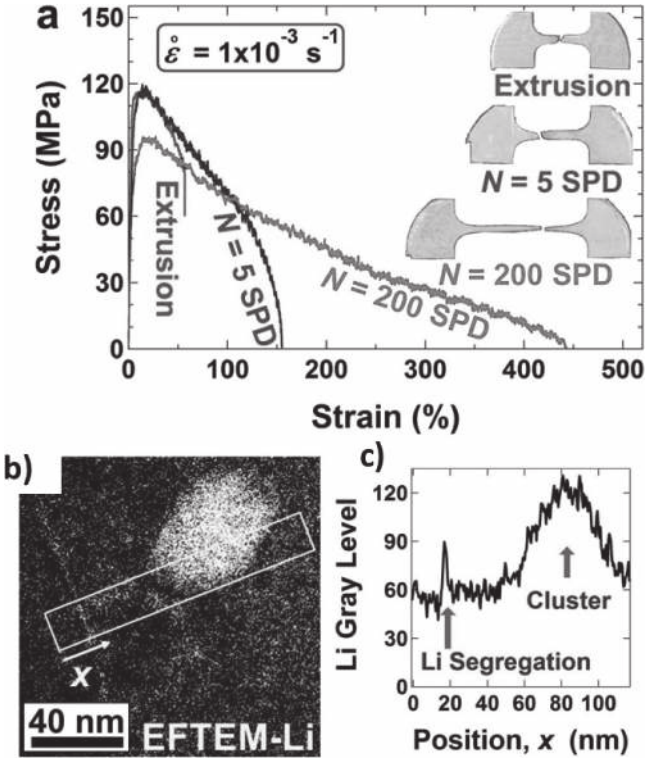


Fig. 7 (a) Room temperature stress-strain curves of a UFG Mg8%Li alloy achieved by SPD (N refers to the number of HPT revolutions); (b) and (c) EFTEM data for the material "N = 200 SPD" showing a Li nanoscaled cluster and Li segregation at a GB that promotes the room temperature superplasticity (reproduced from Ref. 76 with permission from Nature Publishing Group).

In UFG alloys processed by SPD, the influence of GB segregations on strength has also been considered[14,20] and there are several experimental evidences of such correlation, like in 5### aluminum alloys,[44] Al5Cu[71] and 316 stainless steel.[46,72,73] In such steels, APT analyses have helped indeed to prove that strain induced GB segregations of Si (and in lower proportion of Mo and Cr) occur during SPD at 400°C (Fig. 6(a)). Then, even if the grain size is significantly larger as compared to the material processed in similar condition at room temperature (90 nm vs 40 nm), the yield stress is relatively unchanged and is about 1.7 GPa in both cases (Fig. 6(b)). It has been then proposed that the critical stress necessary to nucleate dislocations from boundaries is significantly increased by solutes lying at GBs.[46]

GB segregations do not only affect the yield stress but may also have a significant impact on the plastic behavior[85] and especially as soon as superplastic properties are concerned. Indeed, the underlying mechanisms of superplasticity are connected with grain boundary sliding (GBS) which is directly linked to GB structures and GB diffusion coefficients.[74] The Al–Zn system is well known for its potential superplastic properties when the grain size is in the UFG regime,[75] and it has been shown that Zn GB segregations facilitate GBS even at room temperature.[40] In Mg–Li alloys that have also been developed for superplastic properties, processing by SPD leads to grain refinement which significantly enhances the plastic behavior at room temperature ($0.35\,T_m$).[76] It is however interesting to note that a 440% elongation at room temperature is only achieved for a relatively large number of HPT revolutions (Fig. 7(a)). Thanks to Energy Filtered TEM (EFTEM) it has been demonstrated that this unusual behavior is directly connected to the strain induced formation of Li rich layers at GBs (Fig. 7(b)).[76]

### 4.2 Influence of strain induced segregations on thermal stability

As soon as potential applications of UFG materials are concerned, the thermal stability is a major concern. Indeed, in such materials the driving force for grain growth is intrinsically large, thus if enough mobility is provided, grains will coarsen and the mechanical strength decreases. However, an enhanced thermal stability could be achieved if GBs are pinned by particles (so-called Zener pinning)[58] or segregations.[25] Besides, equilibrium GB segregations are driven by a minimization of the GB energy, thus they could help also stabilizing UFG or nanocrystalline structures by reducing the driving force for grain growth.[28–32,77–80] It is also interesting to note that as reported for nickel processed by HPT, only a small amount of impurities might significantly shift the temperature where a hardness drop (attributed to grain growth) is experimentally observed.[20,21]

In some precipitation hardening alloys, like in 7### or 6### aluminum alloys, strain induced GB segregations could affect the precipitation mechanisms during thermal aging.[38,81] The main reason comes from GBs which are enriched in solute and which are easy nucleation sites (the

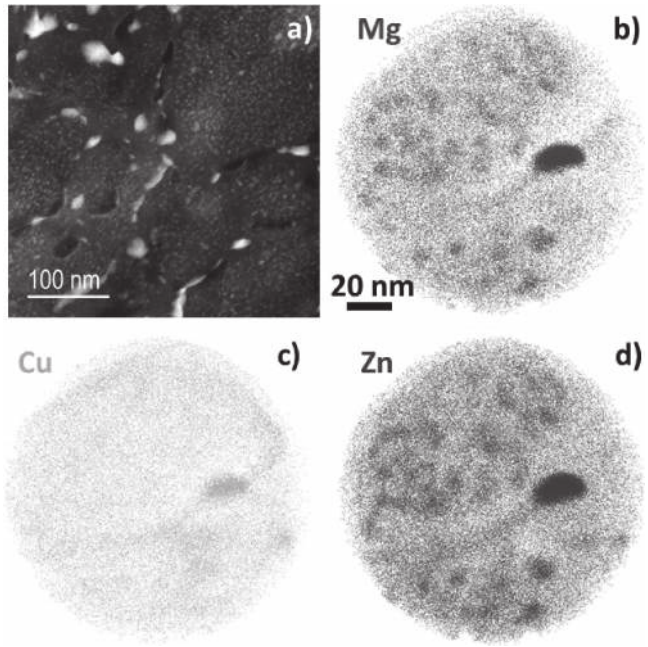


Fig. 8 7449 Aluminum alloy processed by HPT at RT (shear strain ~ 300) and aged 48 h at 100°C. STEM HAADF image showing heterogeneous precipitation at GBs and intragranular precipitation (a), section of a 3D reconstruction of a volume analyzed by APT showing the nanoscaled intragranular precipitates and a bigger precipitate lying at a GB (Mg (b), Cu (c) and Zn (d)).

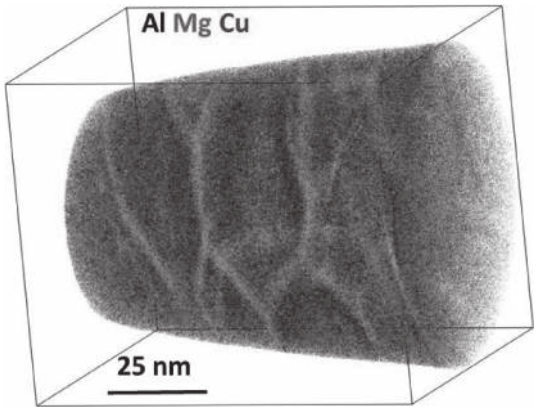


Fig. 9 3D reconstruction of a volume ($88 \times 88 \times 110\,nm^3$) analyzed by APT in a 2024 Aluminum alloy processed by HPT at RT (shear strain ~ 300) and aged at 150°C. Al atoms are displayed in blue, Mg atoms in green and Cu atoms in red. It clearly exhibit intensive GB segregation and stabilization of the UFG structure resulting from SPD.

nucleation barrier is locally lowered). Then, in aluminum alloys, it usually leads to the heterogeneous nucleation of stable phases at GBs instead of the complex sequence of homogeneous precipitation of metastable phases.[82,83] This typical feature is illustrated on Fig. 8, where on the HAADF image (Fig. 8(a)) large precipitates are clearly exhibited at GBs, nanoscaled precipitates inside the grains and a precipitate free zone (dark layer) also appears near GBs. Such typical nanoscaled structure, directly resulting from grain refinement and segregations induced by SPD, is also imaged by APT where the two different kinds of precipitates are clearly exhibited (Fig. 8(a), 8(b) and 8(c)).

There are also some situations where precipitation is not observed but instead segregations become more pronounced. This is the case of the 2024 aluminum alloy deformed by HPT (Fig. 9), where low temperature annealing enhances GB segregations but does not lead to intensive precipitation. This could be the result of the relatively high stability of GB segregations as compared to the driving force for precipitation. It is also interesting to note that in an Al–5Cu alloy processed by ECAP, both mechanisms have been reported, namely simultaneous precipitation and GB segregation during low temperature annealing.[71] Thus, in precipitation hardening aluminum alloys, the thermal stability of the UFG structure achieved by means of SPD is deeply influenced by strain induced GB segregations and could be dependent of various factors such as the processing route, the annealing temperature and the chemical composition of the alloy. This complexity makes any prediction rather difficult but on the other hand it opens the way to a large room for microstructure optimization. In Fe and Ni based alloys, enhancement of GB segregations during short time or low temperature annealing has also been reported.[46,66,68,72,73,84] As soon as the grain size does not grow dramatically, it is interesting to note that it is often connected with a significant strengthening. As discussed in the previous section, it is most probably the result of a higher critical stress necessary to nucleate dislocations at GBs in UFG alloys when some solutes occupy lattice sites at GBs.

## 5. Conclusions

(1) Solute atoms and impurities play a key role in the grain refinement mechanisms as they strongly influence the dynamic recovery processes.
(2) Strain induced GB segregations have been revealed in various metallic alloys processed by SPD. Their characterization and quantitative analysis usually requires analytical transmission electron microscopy and/or atom probe tomography techniques.
(3) Several mechanisms may lead to the formation of strain induced GB segregations during SPD. Solutes and impurities could be dragged by moving dislocations and moving boundaries. There is also a significant contribution of strain induced vacancies that significantly enhance the atomic mobility.
(4) Strain induced GB segregations may promote heterogeneous dynamic precipitation during SPD processing of supersaturated solid solutions, especially because GBs are fast diffusions paths.
(5) It has been experimentally reported in various materials that GB segregations in UFG materials may significantly affect the mechanical properties. For example, they could lead to an enhancement of the yield stress or of superplastic properties.
(6) GB segregations have a strong influence on the thermal stability of UFG alloys. They might reduce the driving force for grain growth or simply provide an efficient pinning of GBs during thermal aging. In precipitate hardening alloys, the precipitation kinetics is often modified and especially extensive heterogeneous precipitation along GBs may occur.

## Acknowledgments

The authors would like to acknowledge the following partners: Dr. Takahiro Masuda, Prof. Zenji Horita, Dr. Kaveh Edalati, Dr. Ivan Lomakin, Dr. Artur Ganeev, Dr. Marina Abramova, Dr. Nariman Enikeev, Dr. Maxim Murashkin, Prof. Ruslan Valiev, Dr. Julia Ivanisenko, Prof. Alexis Deschamps and Dr. Frédéric De Geuser. The present contribution is deeply influenced by our joint projects carried out during the past years and the intense scientific discussions that we had together about materials processed by SPD.

## REFERENCES

1) R.Z. Valiev, Y. Estrin, Z. Horita, T.G. Langdon, M.J. Zehetbauer and Y. Zhu: JOM **58** (2006) 33–39.
2) R.Z. Valiev, M.J. Zehetbauer, Y. Estrin, H.-W. Höppel, Yu. Ivanisenko, H. Hahn, G. Wilde, H.J. Roven, X. Sauvage and T.G. Langdon: Adv. Eng. Mater. **9** (2007) 527–533.
3) R.Z. Valiev, R.K. Islamgaliev and I.V. Alexandrov: Prog. Mater. Sci. **45** (2000) 103–189.
4) N. Hansen: Scr. Mater. **51** (2004) 801–806.
5) Y. Chen, N. Gao, G. Sha, S.P. Ringer and M.J. Starink: Acta Mater. **109** (2016) 202–212.
6) P.V. Liddicoat, X.-Z. Liao, Y. Zhao, Y. Zhu, M.Y. Murashkin, E.J. Lavernia, R.Z. Valiev and S.P. Ringer: Nat. Commun. **1** (2010) 63.
7) I.F. Mohamed, T. Masuda, S. Lee, K. Edalati, Z. Horita, S. Hirosawa, K. Matsuda, D. Terada and M.Z. Omar: Mater. Sci. Eng. A **704** (2017) 112–118.
8) Y. Zhang, S. Jin, P.W. Trimby, X. Liao, M.Y. Murashkin, R.Z. Valiev, J. Liu, J.M. Cairney, S.P. Ringer and G. Sha: Acta Mater. **162** (2019) 19–32.
9) E. Ma: JOM **58** (2006) 49.
10) R. Pippan, S. Scheria, A. Taylor, M. Hafok, A. Hohenwarter and A. Bachmaier: Annu. Rev. Mater. Res. **40** (2010) 319–343.
11) X. Sauvage, G. Wilde, S. Divinsky, Z. Horita and R.Z. Valiev: Mater. Sci. Eng. A **540** (2012) 1–12.
12) Y. Amouyal, S.V. Divinski, L. Klinger and E. Rabkin: Acta Mater. **56** (2008) 5500–5513.
13) Z. Horita and T.G. Langdon: Mater. Sci. Eng. **410–411** (2005) 422.
14) Y. Iwahashi, Z. Horita, M. Nemoto and T.G. Langdon: Metall. Mater. Trans. A **29** (1998) 2503–2510.
15) E. Bruder, P. Braun, H. ur Rehman, R.K.W. Marceau, A.S. Taylor, R. Pippan and K. Durst: Scr. Mater. **144** (2018) 5–8.
16) Yu. Ivanisenko, X. Sauvage, A. Mazilkin, A. Kilmametov, J.A. Beach and B.B. Straumal: Adv. Eng. Mater. **20** (2018) 1800443.
17) X. Sauvage, A. Ganeev, Y. Ivanisenko, N. Enikeev, M. Murashkin and R. Valiev: Adv. Eng. Mater. **14** (2012) 968–974.
18) T. Morishige, T. Hirata, T. Uesugi, Y. Takigawa, M. Tsujikawa and K. Higashi: Scr. Mater. **64** (2011) 355–358.
19) K. Edalati, D. Akama, A. Nishio, S. Lee, Y. Yonenaga, J.M. Cubero-Sesin and Z. Horita: Acta Mater. **69** (2014) 68–77.
20) H.W. Zhang, K. Lu, R. Pippan, X. Huang and N. Hansen: Scr. Mater. **65** (2011) 481–484.
21) H.W. Zhang, X. Huang, R. Pippan and N. Hansen: Acta Mater. **58** (2010) 1698–1707.
22) Y. Ito, K. Edalati and Z. Horita: Mater. Sci. Eng. A **679** (2017) 428–434.
23) O. Renk and R. Pippan: Scr. Mater. **154** (2018) 212–215.
24) O. Renk, P. Ghosh and R. Pippan: Scr. Mater. **137** (2017) 60–63.
25) E. Hersent, K. Marthinsen and E. Nes: Metall. Mater. Trans. A **45** (2014) 4882.
26) X. Sauvage and Y. Nasedkina: Diffus. Found. **5** (2015) 77.
27) R.W. Cahn and P. Haasen (ed.): *Physical Metallurgy*, 4th ed., (North-Holland, Amsterdam, 1996).
28) H.A. Murdoch and C.A. Schuh: J. Mater. Res. **28** (2013) 2154–2163.
29) K.C. Alexander and C.A. Schuh: Scr. Mater. **68** (2013) 937–940.
30) P. Lejcek: *Grain Boundary Segregations in Metals*, (Springer-Verlag, Berlin Heidelberg, 2010).
31) R. Kirchheim: Acta Mater. **55** (2007) 5129–5138.
32) P. Lejček and S. Hofmann: Crit. Rev. Solid State Mater. Sci. **33** (2008) 133–163.
33) W. Lefebvre-Ulrikson, F. Vurpillot and X. Sauvage (ed.): *Atom Probe Tomography, Put Theory into Practice*, (Elsevier, 2016).
34) A.J. Detor, M.K. Miller and C.A. Schuh: Philos. Mag. Lett. **87** (2007) 581–587.
35) M. Herbig, D. Raabe, Y.J. Li, P. Choi, S. Zaefferer and S. Goto: Phys. Rev. Lett. **112** (2014) 126103.
36) G. Sha, Y.B. Wang, X.Z. Liao, Z.C. Duan, S.P. Ringer and T.G. Langdon: Acta Mater. **57** (2009) 3123–3132.
37) G. Sha, L. Yao, X. Liao, S.P. Ringer, Z. Chao Duan and T.G. Langdon: Ultramicroscopy **111** (2011) 500–505.
38) X. Sauvage, E.V. Bobruk, M.Yu. Murashkin, Y. Nasedkina, N.A. Enikeev and R.Z. Valiev: Acta Mater. **98** (2015) 355–366.
39) G. Nurislamova, X. Sauvage, M. Murashkin, R. Islamgaliev and R. Valiev: Philos. Mag. Lett. **88** (2008) 459–466.
40) N.Q. Chinh, R.Z. Valiev, X. Sauvage, G. Varga, K. Havancsák, M. Kawasaki, B.B. Straumal and T.G. Langdon: Adv. Eng. Mater. **16** (2014) 1000–1009.
41) B.B. Straumal, X. Sauvage, B. Baretzky, A.A. Mazilkin and R.Z. Valiev: Scr. Mater. **70** (2014) 59–62.
42) Y. Nasedkina, X. Sauvage, E. Bobruk and M. Murashkin: J. Alloys Compd. **710** (2017) 736–747.
43) X. Sauvage, N. Enikeev, R. Valiev, Y. Nasedkina and M. Murashkin: Acta Mater. **72** (2014) 125–136.
44) R.Z. Valiev, N.A. Enikeev, M.Yu. Murashkin, V.U. Kazykhanov and X. Sauvage: Scr. Mater. **63** (2010) 949–952.
45) M. Murashkin, I. Sabirov, A. Medvedev, N. Enikeev, W. Lefebvre, R. Valiev and X. Sauvage: Mater. Des. **90** (2016) 433–442.
46) M.M. Abramova, N.A. Enikeev, R.Z. Valiev, A. Etienne, B. Radiguet, Y. Ivanisenko and X. Sauvage: Mater. Lett. **136** (2014) 349–352.
47) E. Hug, R. Prasath Babu, I. Monnet, A. Etienne, F. Moisy, V. Pralong, N. Enikeev, M. Abramova, X. Sauvage and B. Radiguet: Appl. Surf. Sci. **392** (2017) 1026–1035.
48) I. Semenova, G. Salimgareeva, G. Da Costa, W. Lefebvre and R. Valiev: Adv. Eng. Mater. **12** (2010) 803.
49) X. Sauvage, G. Wilde and R. Valiev: Mater. Sci. Forum **667–669** (2011) 169–174.
50) X. Sauvage and Y. Ivanisenko: J. Mater. Sci. **42** (2007) 1615–1621.
51) D. Setman, E. Schafler, E. Korznikova and M.J. Zehetbauer: Mater. Sci. Eng. A **493** (2008) 116–122.
52) W. Sprengel, B. Oberdorfer, E.-M. Steyskal and R. Würschum: J. Mater. Sci. **47** (2012) 7921–7925.
53) A.V. Kazantzis, Z.G. Chen and J.Th.M. De Hosson: J. Mater. Sci. **48** (2013) 7399.
54) M. Legros, G. Dehm, E. Arzt and T.J. Balk: Science **319** (2008) 1646–1649.
55) G. Saada: Physica **27** (1961) 657.
56) A. Etienne, B. Radiguet, N.J. Cunningham, G.R. Odette and P. Pareige: J. Nucl. Mater. **406** (2010) 244–250.
57) K.S. Kormout, R. Pippan and A. Bachmaier: Adv. Eng. Mater. **19** (2016) 1600675.
58) A. Duchaussoy, X. Sauvage, K. Edalati, Z. Horita, G. Renou, A. Deschamps and F. De Geuser: Acta Mater. **167** (2019) 89–102.
59) E.V. Bobruk, X. Sauvage, A. Zakirov and N.A. Enikeev: Rev. Adv. Mater. Sci. **55** (2018) 61–68.
60) X. Sauvage, M.Yu. Murashkin, B.B. Straumal, E.V. Bobruk and R.Z. Valiev: Adv. Eng. Mater. **17** (2015) 1821–1827.
61) B. Straumal, B. Baretzky, A. Mazilkin, F. Phillipp, O. Kogtenkova, M. Volkov and R.Z. Valiev: Acta Mater. **52** (2004) 4469–4478.
62) A. Hohenwarter, B. Faller, R. Rashkova and R. Pippan: Philos. Mag. Lett. **94** (2014) 342–350.
63) K. Edalati, R. Miresmaeili, Z. Horita, H. Kanayama and R. Pippan: Mater. Sci. Eng. A **528** (2011) 7301–7305.
64) R.B. Figueiredo, P.H.R. Pereira, M.T.P. Aguilar, P.R. Cetlin and T.G. Langdon: Acta Mater. **60** (2012) 3190–3198.
65) X. Sauvage, S. Lee, K. Matsuda and Z. Horita: J. Alloys Compd. **710** (2017) 199–204.
66) J. Hu, Y.N. Shi, X. Sauvage, G. Sha and K. Lu: Science **355** (2017)

1292–1296.
67) S. Özerinç, K. Tai, N.Q. Vo, P. Bellon, R.S. Averback and W.P. King: Scr. Mater. **67** (2012) 720–723.
68) X.F. Zhang, T. Fujita, D. Pan, J.S. Yu, T. Sakurai and M.W. Chen: Mater. Sci. Eng. A **527** (2010) 2297–2304.
69) D. Zhao, O.M. Løvvik, K. Marthinsen and Y. Li: Acta Mater. **145** (2018) 235–246.
70) J. Schäfer, A. Stukowski and K. Albe: Acta Mater. **59** (2011) 2957–2968.
71) H. Jia, R. Bjørge, L. Cao, H. Song, K. Marthinsen and Y. Li: Acta Mater. **155** (2018) 199–213.
72) H. Wang, I. Shuro, M. Umemoto, H.-H. Kuo and Y. Todaka: Mater. Sci. Eng. A **556** (2012) 906–910.
73) O. Renk, A. Hohenwarter, K. Eder, K.S. Kormout, J.M. Cairney and R. Pippan: Scr. Mater. **95** (2015) 27–30.
74) T.G. Langdon: Acta Metall. Mater. **42** (1994) 2437–2443.
75) R.Z. Valiev, M.Yu. Murashkin, A. Kilmametov, B. Straumal, N.Q. Chinh and T.G. Langdon: J. Mater. Sci. **45** (2010) 4718–4724.
76) K. Edalati, T. Masuda, M. Arita, M. Furui, X. Sauvage, Z. Horita and R.Z. Valiev: Sci. Rep. **7** (2017) 2662.
77) M.-R. He, S.K. Samudrala, G. Kim, P.J. Felfer, A.J. Breen, J.M. Cairney and D.S. Gianola: Nat. Commun. **7** (2016) 11225.
78) A.J. Detor and C.A. Schuh: Acta Mater. **55** (2007) 4221–4232.
79) A. Devaraj, W. Wang, R. Vemuri, L. Kovarik, X. Jiang, M. Bowden, J.R. Trelewicz, S. Mathaudhu and A. Rohatgi: Acta Mater. **165** (2019) 698–708.
80) P.R. Cantwell, M. Tang, S.J. Dillon, J. Luo, G.S. Rohrer and M.P. Harmer: Acta Mater. **62** (2014) 1–48.
81) H. Zhao, F.D. Geuser, A.K. da Silva, A. Szczepaniak, B. Gault, D. Ponge and D. Raabe: Acta Mater. **156** (2018) 318–329.
82) G. Sha, K. Tugcu, X.Z. Liao, P.W. Trimby, M.Y. Murashkin, R.Z. Valiev and S.P. Ringer: Acta Mater. **57** (2009) 3123–3132.
83) A. Deschamps, F. De Geuser, Z. Horita, S. Lee and G. Renou: Acta Mater. **66** (2014) 105–117.
84) M.M. Abramova, N.A. Enikeev, X. Sauvage, A. Etienne, B. Radiguet, E. Ubyivovk and R.Z. Valiev: Rev. Adv. Mater. Sci. **43** (2015) 83–88.
85) I.A. Ovid'ko, R.Z. Valiev and Y.T. Zhu: Prog. Mater. Sci. **94** (2018) 462–540.